

Shears bands in ^{193}Pb

G. Baldsiefen,¹ M. A. Stoyer,² J. A. Cizewski,¹ D. P. McNabb,¹ W. Younes,¹ J. A. Becker,² L. A. Bernstein,² M. J. Brinkman,² L. P. Farris,² E. A. Henry,² J. R. Hughes,² A. Kuhnert,² T. F. Wang,² B. Cederwall,³ R. M. Clark,³ M. A. Deleplanque,³ R. M. Diamond,³ P. Fallon,³ I. Y. Lee,³ A. O. Macchiavelli,³ J. Oliveira,³ F. S. Stephens,³ J. Burde,³ D. T. Vo,⁴ and S. Frauendorf⁵

¹Rutgers University, New Brunswick, New Jersey 08903

²Lawrence Livermore National Laboratory, Livermore, California 94550

³Lawrence Berkeley Laboratory, Berkeley, California 94720

⁴Iowa State University, Ames, Iowa 50011

⁵Forschungszentrum Rossendorf, D-01314 Dresden, Germany

(Received 25 April 1996)

Four bands of enhanced dipole transitions, with weak crossovers, have been observed in ^{193}Pb . Three of these bands are connected to the spherical levels. In addition, the spherical level scheme has been extended. The nuclear spectroscopy was done with the early implementation of GAMMASPHERE and HERA arrays of Ge detectors. The nucleus ^{193}Pb was populated in the $^{174}\text{Yb}(^{24}\text{Mg},5n)$ reaction at beam energies of 129, 131, and 134 MeV. The experimental results are compared to tilted-axis cranking calculations. The systematical behavior of the dipole bands in the heavier odd- A Pb isotopes, $^{195,197,199,201}\text{Pb}$, is also discussed. [S0556-2813(96)06409-6]

PACS number(s): 21.10.Hw, 21.60.-n, 23.20.-g, 27.80.+w

I. INTRODUCTION

Sequences of enhanced magnetic dipole bands have recently been discovered in more than 20 isotopes in the lead region [1–16]. All of these sequences show similar properties. They consist of strong magnetic dipole transitions with weak $E2$ crossover transitions. Despite the small nuclear deformations deduced from lifetime measurements [17–21], the bands have fairly regular energy spacings and show no or only small signature splitting up to the highest rotational frequencies.

The bands are understood as being built on configurations involving the high- K proton $h_{9/2}$ and $i_{13/2}$ orbitals and holes in the low- K orbitals of the $i_{13/2}$ neutron shell. Therefore, near the bandhead the angular momentum of the protons is aligned along the symmetry axis, while the angular momentum of the neutrons is aligned perpendicular to the symmetry axis. Hence, the direction of the total angular momentum is tilted by an angle of about 45° with respect to the symmetry axis.

A striking feature of these $M1$ bands is that the ratio of the dynamic moment-of-inertia to the $B(E2)$ value is about ten times larger than in well deformed nuclei. This indicates that part of the moment-of-inertia stems from sources other than collective rotation. Recently, the characteristics of these bands with enhanced $M1$ transitions have been successfully interpreted in terms of the tilted axis cranking model [22,23]. In this model the increase in the angular momentum within the bands is created by the increase in the alignment of the proton and the neutron spins in the direction of the total spin. Since the change in the neutron and proton spin vectors is similar to the closing of the blades of a pair of shears, the term “shears bands” was suggested for these $M1$ bands.

II. EXPERIMENTS

The experiment was performed at the 88-Inch Cyclotron Facility at Lawrence Berkeley National Laboratory. Data

were collected using initially the High Energy Resolution Array (HERA) and, subsequently, early implementation of Gammasphere. The reaction was $^{174}\text{Yb}(^{24}\text{Mg},5n)$ at beam energies of 131 MeV (Gammasphere) and 129 and 134 MeV (HERA). The targets consisted of a stack of three self-supporting foils each with a thickness of ~ 0.5 mg/cm². The HERA experiments involved 20 Compton-suppressed Ge detectors ($\sim 25\%$ efficient with respect to a 7.5 cm \times 7.5 cm NaI detector at 25 cm) and a 40-element bismuth-germanate (BGO) inner ball. The numbers (angles with respect to the beam direction) of the Ge detectors were: 4(37°), 2(51°), 4(79°), 2(103°), 4(123°), 2(152°), and 2(154°). Each detector was 15.5 cm from the target. The Gammasphere experiment involved 36 Compton-suppressed Ge detectors with $\sim 80\%$ efficiency. Six detectors were placed at 90° , and five each at 17° , 32° , 37° , 143° , 148° , and 163° with respect to the beam direction. All of these detectors were located 25 cm from the target. The HERA data set consisted of 160×10^6 and 310×10^6 γ - γ coincidences at 129 and 134 MeV, respectively. The Gammasphere data set consisted of 5×10^8 three- and higher-fold events, yielding 9×10^8 unfolded γ - γ - γ coincidences.

The HERA data were sorted into symmetrized γ - γ matrices and forward/backward vs 90° matrices for a directional correlation analysis (DCO). A preliminary level scheme [24], including levels up to $E_{\text{ex}} \approx 5$ MeV and $I \approx 45/2\hbar$, was obtained using coincidence relationships, relative γ -ray intensities and ΔI spin measurements from DCO ratios.

The Gammasphere data were sorted [25] into a symmetrized three-dimensional cube and the level scheme was extended to $E_{\text{ex}} = 7.0$ MeV and $I = 55/2\hbar$. A DCO matrix was generated with the 90° detectors on one axis and the forward plus backward detectors on the other axis. DCO ratios were determined by setting gates on clean strong transitions on both axes. The DCO ratios were normalized to known $E2$

TABLE I. Gamma-ray intensities, DCO ratios and assignments for dipole bands in ^{193}Pb .

E_γ (keV)	I_γ ^a	R_{DCO} ^b	$I_i \rightarrow I_f$
Band 1a			
102.5	3.4 ± 0.8		$31/2^- \rightarrow 29/2^-$
252.3	19.4 ± 3.9	0.50 ± 0.10	$33/2^- \rightarrow 31/2^-$
334.4	3.5 ± 0.9	0.51 ± 0.07	$41/2^- \rightarrow 39/2^-$
353.3	1.4 ± 0.6	0.59 ± 0.12	$45/2^- \rightarrow 43/2^-$
357.4	2.9 ± 0.9	0.49 ± 0.07	$43/2^- \rightarrow 41/2^-$
381.2	18.5 ± 3.9	0.48 ± 0.05	$35/2^- \rightarrow 33/2^-$
401.3	11.1 ± 2.4	0.48 ± 0.05	$37/2^- \rightarrow 35/2^-$
413.3	6.8 ± 1.6	0.50 ± 0.06	$39/2^- \rightarrow 37/2^-$
633.2	1.4 ± 0.5		$35/2^- \rightarrow 31/2^-$
691.7	0.3 ± 0.1		$43/2^- \rightarrow 39/2^-$
710.7	0.4 ± 0.2		$45/2^- \rightarrow 41/2^-$
747.6	0.5 ± 0.2		$41/2^- \rightarrow 37/2^-$
782.5	2.8 ± 0.7	1.09 ± 0.21	$37/2^- \rightarrow 33/2^-$
814.5	3.0 ± 0.9		$39/2^- \rightarrow 35/2^-$
Band 1b			
239.1	1.0 ± 0.6		$(49/2 \rightarrow 47/2)$
265.1	1.6 ± 0.9		$(51/2 \rightarrow 49/2)$
329.4	1.1 ± 0.7		$(53/2 \rightarrow 51/2)$
374.9	0.4 ± 0.3		$(55/2 \rightarrow 53/2)$
Band 2			
197.0	2.0 ± 0.8	0.52 ± 0.16	$(41/2 \rightarrow 39/2)$
232.0	5.5 ± 1.7	0.44 ± 0.12	$(43/2 \rightarrow 41/2)$
291.4	5.6 ± 1.8	0.52 ± 0.10	$(45/2 \rightarrow 43/2)$
365.0	4.3 ± 1.4	0.53 ± 0.09	$(47/2 \rightarrow 45/2)$
389.1	2.5 ± 0.8	0.53 ± 0.11	$(49/2 \rightarrow 47/2)$
415.7	1.6 ± 0.6	0.54 ± 0.12	$(51/2 \rightarrow 49/2)$
425.7	0.9 ± 0.4	0.50 ± 0.13	$(53/2 \rightarrow 51/2)$
432.3	0.6 ± 0.3		$(55/2 \rightarrow 53/2)$
753.8	0.9 ± 0.3		$(49/2 \rightarrow 45/2)$
Band 3			
342.6	6.4 ± 1.2	0.48 ± 0.07	$29/2^+ \rightarrow 27/2^+$
363.5	4.7 ± 1.0	0.41 ± 0.07	$31/2^+ \rightarrow 29/2^+$
381.7	1.5 ± 0.5	0.38 ± 0.08	$35/2^+ \rightarrow 33/2^+$
409.3	2.2 ± 0.5	0.40 ± 0.08	$33/2^+ \rightarrow 31/2^+$
705.9	1.7 ± 0.4		$31/2^+ \rightarrow 27/2^+$
772.8	1.5 ± 0.4		$33/2^+ \rightarrow 29/2^+$
791.1	1.2 ± 0.3		$35/2^+ \rightarrow 31/2^+$

^aGamma-ray intensities are normalized to the 881-keV $17/2^+ \rightarrow 13/2^+$ transition.

^bDCO ratios are normalized to $E2$ quadrupole transitions.

transitions, as well as $E2$ transitions determined in the analysis of the HERA data. All DCO ratios were obtained in several gates and the average values are given in Tables I and II. Below 300 keV in γ -ray energy the DCO errors are dominated by large uncertainties in the efficiency calibration at low energy.

Intensities of the transitions have been determined by fitting a one-dimensional projection spectrum of the γ - γ - γ coincidences and are summarized in Tables I and II. The intensities of weak lines were determined from coincidence spectra and are normalized using strong reference transitions.

III. EXPERIMENTAL RESULTS

High-spin levels in ^{193}Pb were studied for the first time by Lagrange *et al.* [26]. In this earlier work 21 γ -ray transitions were found, and conversion coefficients, angular distributions, and lifetimes of the isomers were measured. In the present work 20 of the 21 earlier transitions were confirmed. We have been able to place 90 new transitions in the level scheme. Several of these form three regular and one short, less regular $M1$ dipole bands. The level scheme is rather complex and was, therefore, divided into three parts (Figs. 1, 2, and 3). For a better orientation the remaining levels are organized as groups of states. As explained below, some of the groups show properties similar to those of the bands. Therefore, the subdivision into bands and groups should not be taken as an absolute measure. In Fig. 1 the lines of groups 1, 3, and 4 (with the exception of the 432 keV transition of group 1) represent the earlier known lines [26]. Also, the two strongest lines of band 1a (at 252 and 381 keV) had been found earlier in Ref. [26]. Intensities and DCO ratios of all transitions are given in Tables I and II.

Gamma-ray energies have been corrected for the nonlinearity of the analog-to-digital converters (ADC's) in the present measurements. However, there remain differences of about 0.5 keV in the medium energy range compared to the earlier work of Ref. [26]. In both works the transition energy sums are correct to ± 0.4 keV.

A. Irregularly spaced, spherical levels

To facilitate the discussion, the levels not assigned to the dipole bands have been divided into several groups as illustrated in Figs. 1, 2 and 3. The transitions in band 1 are in coincidence with the spherical transitions of group 1, while band 2 decays to the group 2 of levels. The remaining spherical levels are divided somewhat arbitrarily into groups 3 and 4. The transitions of group 5 feed band 1a.

From the systematics we have estimated the excitation energy of the $13/2^+$ isomer in group 1 to be ≈ 100 keV. In the figures and tables of the present work the energy of the $13/2^+$ isomer is defined to be zero. Its lifetime is taken from [27]. The low-energy transition which feeds the 2140-keV level in Fig. 1 was not observed in our experiments due to low efficiency of the Ge detectors at this energy. Its transition energy was determined by the energy difference of the 811.7 and 739.0-keV lines, which gives 72.7 keV, within errors of the value found by Ref. [26]. The spins and parities of the levels in group 1 are taken from [26] and spins are confirmed by our DCO ratios.

Group 2 in Fig. 1 represents the transitions which connect band 2 to the low-lying levels. The transitions below the 3837-keV level in Fig. 1 are relatively strong. The DCO ratios of the 310, 555, 296 and 462-keV transitions are consistent with $\Delta I = 1$ dipole transitions, while the DCO ratios for the 851 and 758-keV transitions are in agreement with $\Delta I = 2$ quadrupole transitions. The spin of the 3837-keV level is, therefore, estimated to be $33/2$. There remains a small ambiguity in the spin assignment, since the DCO ratios of all of the lines in group 2 cannot exclude mixed $M1 + E2$ $\Delta I = 0$ or $\Delta I = 1$ assignments. Nevertheless the spins are sufficiently trustworthy to allow a definite, rather than tentative,

TABLE II. Gamma-ray intensities and DCO ratios for normal transitions in ^{193}Pb .

E_γ (keV)	I_γ^a	R_{DCO}^b	$E_i \rightarrow E_f$
Group 1			
72.7			2212 \rightarrow 2140
158.4	28.0 ± 4.0	0.67 ± 0.20	2584 \rightarrow 2426
213.0	23.0 ± 3.4	0.60 ± 0.17	2426 \rightarrow 2212
219.1	4.2 ± 1.0	1.04 ± 0.26	2212 \rightarrow 1993
431.9	1.7 ± 0.7	0.59 ± 0.14	2426 \rightarrow 1993
519.6	81.8 ± 9.6	0.96 ± 0.11	1401 \rightarrow 881
527.3	10.2 ± 1.9	1.05 ± 0.15	1549 \rightarrow 1022
590.6	30.0 ± 5.7	0.97 ± 0.15	2140 \rightarrow 1549
592.5	35.4 ± 8.8	1.08 ± 0.14	1993 \rightarrow 1401
668.0	9.0 ± 1.7	0.58 ± 0.07	1549 \rightarrow 881
739.0	18.8 ± 4.0	0.58 ± 0.07	2140 \rightarrow 1401
811.7	9.8 ± 1.9	0.91 ± 0.12	2212 \rightarrow 1401
881.3	100.0 ± 11.3	0.96 ± 0.11	881 \rightarrow 0
1022.1	12.2 ± 2.1	0.77 ± 0.14	1022 \rightarrow 0
Group 2			
97.7	2.2 ± 0.8		2523 \rightarrow 2426
146.4	4.8 ± 1.8	0.48 ± 0.21	4148 \rightarrow 4001
148.7	4.5 ± 2.3	0.53 ± 0.18	4297 \rightarrow 4148
164.3	7.5 ± 2.1	0.51 ± 0.16	4001 \rightarrow 3837
224.3	1.7 ± 0.8		5168 \rightarrow 4943
279.1	3.4 ± 1.3		4576 \rightarrow 4297
296.3	4.9 ± 1.5	0.53 ± 0.11	3375 \rightarrow 3078
310.8	9.9 ± 1.9	0.63 ± 0.13	2523 \rightarrow 2212
367.8	2.5 ± 1.0		4943 \rightarrow 4576
395.4	5.5 ± 1.7		3770 \rightarrow 3375
438.3	2.1 ± 0.8		4208 \rightarrow 3770
462.6	13.0 ± 3.3	0.49 ± 0.07	3837 \rightarrow 3375
555.0	6.6 ± 2.3	0.52 ± 0.07	3078 \rightarrow 2523
758.9	2.3 ± 0.9	1.16 ± 0.31	3837 \rightarrow 3078
851.3	16.0 ± 5.4	0.96 ± 0.14	3375 \rightarrow 2523
Group 3			
85.5			2610 \rightarrow 2525
447.6	0.9 ± 0.3		3860 \rightarrow 3412
531.5	3.8 ± 1.1	0.93 ± 0.17	2525 \rightarrow 1993
539.5	1.8 ± 1.2		3904 \rightarrow 3365
581.4	0.8 ± 0.3		4441 \rightarrow 3860
632.2	1.3 ± 0.9		4239 \rightarrow 3607
644.0	0.6 ± 0.3		4757 \rightarrow 4113
677.0	9.9 ± 1.9	0.93 ± 0.11	2670 \rightarrow 1993
701.2	1.6 ± 0.5		4113 \rightarrow 3412
741.9	4.5 ± 1.2	0.97 ± 0.17	3412 \rightarrow 2670
754.4	5.6 ± 3.0		3365 \rightarrow 2610
996.5	3.0 ± 1.8		3607 \rightarrow 2610
Group 4			
180.2	12.1 ± 2.9	0.61 ± 0.16	2321 \rightarrow 2141
184.3	19.5 ± 3.0	1.07 ± 0.28	1585 \rightarrow 1401
301.6	1.8 ± 0.6		2705 \rightarrow 2404
331.3	0.5 ± 0.3		2652 \rightarrow 2321
340.7	1.9 ± 0.6		2993 \rightarrow 2652
384.4	1.5 ± 0.7		2705 \rightarrow 2321
421.2	4.4 ± 1.3	0.89 ± 0.17	3127 \rightarrow 2705
472.1	4.8 ± 1.4	0.46 ± 0.13	2057 \rightarrow 1585

TABLE II. (*Continued*)

E_γ (keV)	I_γ^a	R_{DCO}^b	$E_i \rightarrow E_f$
542.2	2.8 ± 1.0		3247 \rightarrow 2705
546.3	6.4 ± 1.7	1.11 ± 0.17	3539 \rightarrow 2993
555.5	29.5 ± 9.4	0.77 ± 0.09	2141 \rightarrow 1585
564.6	7.2 ± 1.9	0.89 ± 0.15	2705 \rightarrow 2141
594.3	2.6 ± 1.3		2652 \rightarrow 2057
612.6	8.3 ± 2.2	0.96 ± 0.13	3739 \rightarrow 3127
638.3	3.2 ± 1.0	1.13 ± 0.19	4177 \rightarrow 3539
647.5	1.3 ± 0.5		4634 \rightarrow 3987
655.7	1.9 ± 0.8		4395 \rightarrow 3739
672.0	6.9 ± 1.8	1.09 ± 0.15	2993 \rightarrow 2321
692.8	3.2 ± 1.0	0.89 ± 0.15	4432 \rightarrow 3739
711.5	0.7 ± 0.4		4889 \rightarrow 4177
729.3	1.5 ± 0.6	0.97 ± 0.30	5162 \rightarrow 4432
739.5	1.8 ± 0.6		3987 \rightarrow 3247
766.5	0.8 ± 0.4		5162 \rightarrow 4395
805.9	8.8 ± 2.2	0.91 ± 0.11	3127 \rightarrow 2321
819.0	3.3 ± 1.0		2404 \rightarrow 1585
Group 5			
302.8	1.0 ± 0.4	0.45 ± 0.12	4469 \rightarrow 4166
319.5	2.4 ± 0.8	0.53 ± 0.10	3639 \rightarrow 3320
415.3	1.9 ± 1.0		4055 \rightarrow 3639
423.3	1.3 ± 0.5	0.44 ± 0.09	4589 \rightarrow 4166
441.7	1.0 ± 0.4		5031 \rightarrow 4589
444.4	3.4 ± 1.1	0.46 ± 0.08	4166 \rightarrow 3721
454.6	0.7 ± 0.4		4589 \rightarrow 4135
482.5	1.9 ± 0.9	0.45 ± 0.08	4537 \rightarrow 4055
834.0	2.8 ± 1.3		3418 \rightarrow 2584
845.8	1.1 ± 0.5		4166 \rightarrow 3320
867.8	1.2 ± 0.5		4589 \rightarrow 3721

^aGamma-ray intensities are normalized to the 881-keV transition.

^bDCO ratios are normalized to $E2$ quadrupole transitions.

character in Fig. 1. The parity of the levels in group 2 cannot be determined because the electric vs magnetic character of the 97 and 310-keV lines which depopulate the 2523-keV level cannot be uniquely determined. The ordering of the 146.4, 148.7, and 164.3-keV lines above the 3837-keV level could not be firmly established. However, this uncertainty has no influence on the excitation energy and spin of band 2. The DCO ratios of all three lines are consistent with $\Delta I = 1$ dipole transitions, therefore, suggesting a spin of 39/2 for the 4297-keV bandhead. However, again mixed $\Delta I = 0$ transitions cannot be completely excluded. Intensity arguments lead to the conclusion that none of the lines at 146.4, 148.7 and 164.3 keV can be magnetic dipoles, because $M1$ transitions are mainly converted at these low energies. The intensity and also the DCO ratio of the 148.7-keV line could only be roughly determined, as it is coincident with an additional line with a transition energy of ≈ 149 keV which is not placed in the level scheme. There are additional weak lines in the upper part of group 2 which could not be placed. Therefore, only tentative spin assignments have been made for levels above 3837 keV. Although the levels of group 2 are irregularly spaced, it is not clear that this group belongs to the spherical part of the level scheme. As is the case for the $M1$ bands, this group consists of dipole transitions with

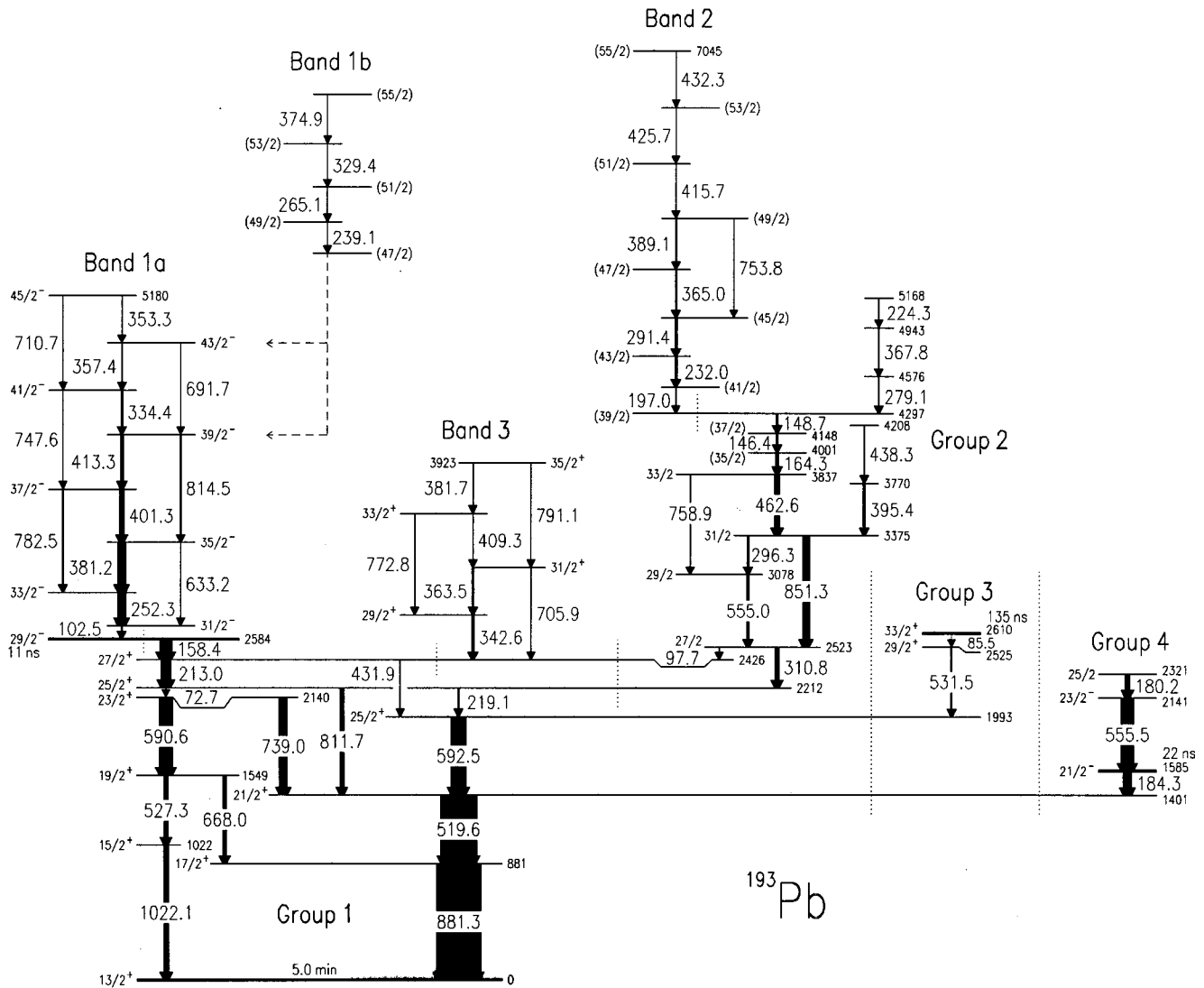


FIG. 1. Partial level scheme of ^{193}Pb . Lifetimes of the $21/2^-$, $29/2^-$, and $33/2^+$ isomers are taken from [26]. The lifetime of the $13/2^+$ isomer is taken from [27]. The widths of the arrows are proportional to the γ -ray intensities. The strongest lines of groups 1, 3, and 4 are included in both parts of the level scheme (Figs. 1 and 2). To aid the reader, the groups and bands shown in Figs. 1, 2, and 3 are separated by dotted lines.

$E2$ crossover transitions. Similar structures have been found, e.g. in ^{194}Pb (groups a, b, and d of Ref. [15]), ^{197}Pb (group 2 of Ref. [16]), ^{198}Pb (group b of Ref. [12]), and ^{200}Pb (group 1 of Ref. [23]).

The transitions of groups 3 and 4 in Fig. 2 extend the spherical level scheme. While none of these transitions are in coincidence with any of the dipole bands, this part of the level scheme might be of interest in the search for transitions which could link the superdeformed bands found in ^{193}Pb [28] to normal excitations. The lifetimes, spins and parities of the levels of groups 3 and 4 displayed in Fig. 1 are taken from [26]. Our DCO ratios confirm the spin assignments given in [26] with the exception of the 2321 level in group 4. Our analysis gives a DCO ratio of 0.61 ± 0.16 for the 180-keV transition depopulating this level, which is not in agreement with the earlier proposed assignment of a stretched quadrupole transition. For most of the 32 new transitions in Fig. 2, DCO ratios could be determined. While many of the new transitions have DCO ratios consistent with stretched

quadrupole character, $\Delta I = 0$ dipole or mixed multiplicities could not be excluded for all of these.

Figure 3 shows the transitions of group 5 which are feeding into band 1a. Most of these γ rays have transition energies near 400 keV (dipoles) and 800 keV ($E2$), as do the transitions in dipole band 1a. Also, the DCO ratios of the group 5 lines are comparable to those of the in-band $M1$ transitions. While the levels in this group have irregular spacings, their properties seem to be closer to those of the regular bands than to the spherical part of the level scheme.

B. Dipole bands

The strongest dipole band observed in the present study has been labeled band 1a in Fig. 1. The characteristics of this band, when combined with its proposed extension, band 1b, are similar to those observed for the strongest negative-parity dipole bands in the heavier odd-mass lead isotopes $^{195,197,199,201}\text{Pb}$ [16,23,29,30]. The second strongest band was

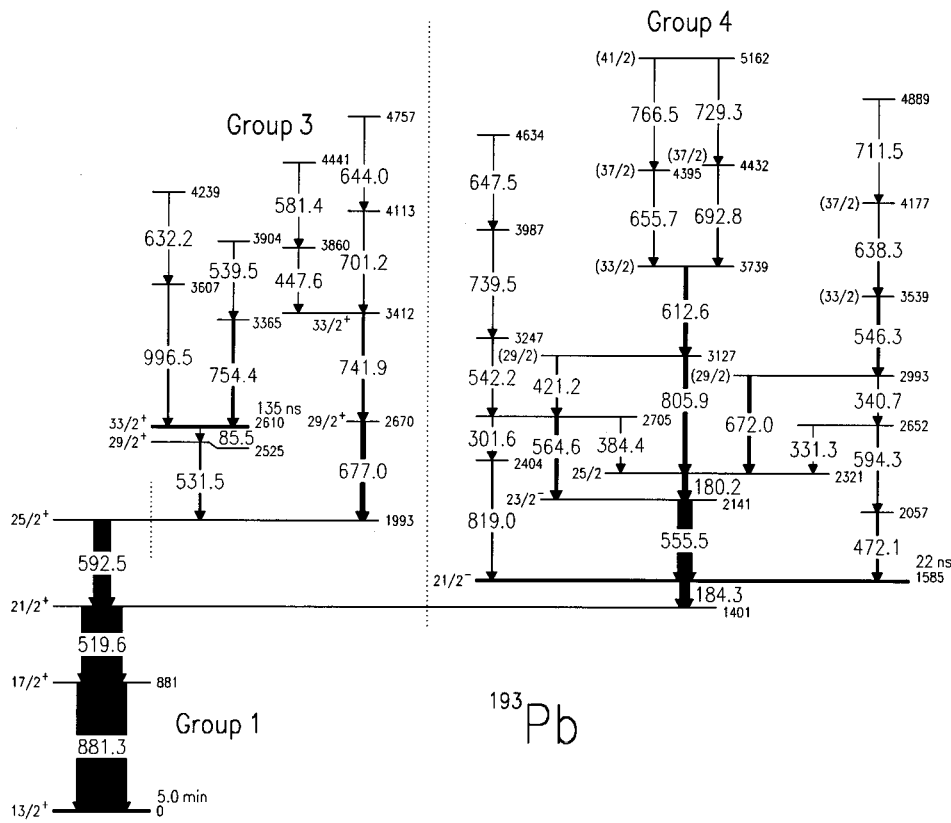


FIG. 2. Partial level scheme of ^{193}Pb showing the spherical part which is not connected to the dipole bands.

labeled band 2. This band is similar to the strongest positive-parity dipole bands in the heavier odd- A lead isotopes [16,23,29,30]. The bands 1a, 1b, 2, and 3 have been populated with 35 ± 6 , 3 ± 2 , 11 ± 3 , and $10 \pm 2\%$ of the intensity of the 881.3-keV transition, respectively.

Figure 4(a) shows a sum of spectra double-gated on the dipole transitions of band 1a. These transitions are in coincidence with transitions in group 1 of the spherical levels. Six weak $E2$ crossover transitions have been found in band 1a. Since the connection to the ground state has been estab-

lished, the spin and excitation energy of the bandhead are known quantities, which are essential for a comparison between theoretical and experimental values. The DCO ratios of all of the transitions in the cascade are consistent with stretched dipole character. Intensity arguments require an $M1$ assignment for the lowest energy lines. The crossover $E2$ transitions then require all of the levels in the band to have the same parity. The conversion corrected intensities of transitions depopulating the excitations of band 1 are listed in Table III, where the crossover transitions are included in

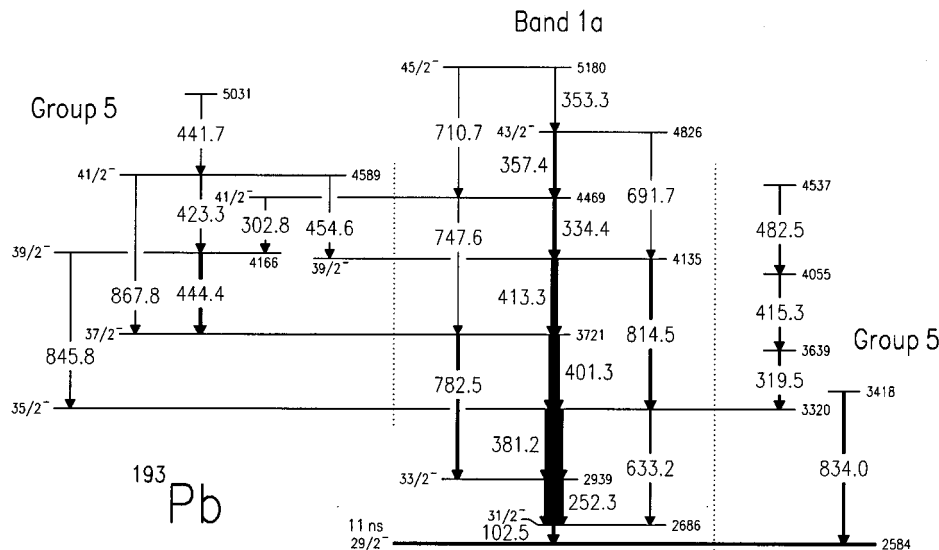


FIG. 3. Partial level scheme of ^{193}Pb showing band 1a and the transitions of group 5 which feed this band.

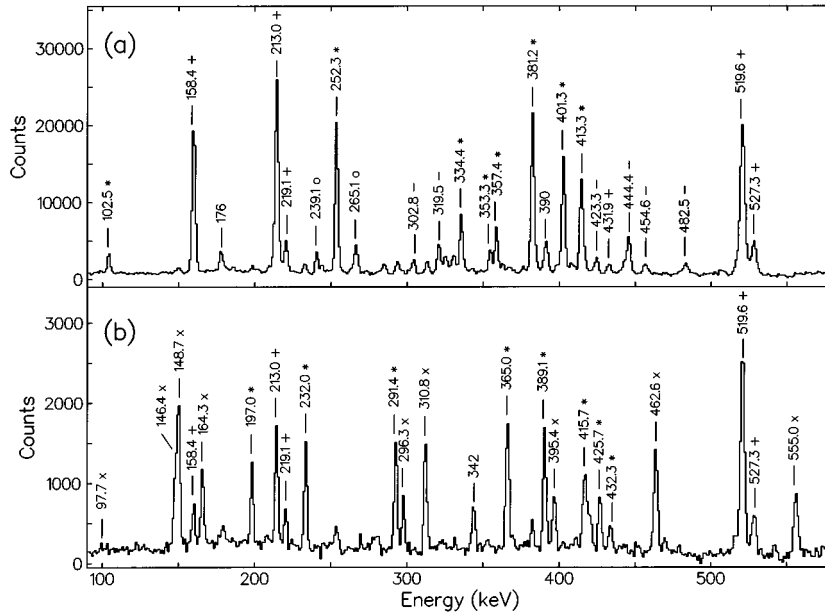


FIG. 4. Sum of double-gated coincidence spectra of bands 1 and 2 in ^{193}Pb . Transitions of bands 1a and 2 are labeled by an asterisk, transitions of band 1b with circles. The transitions within the groups in ^{193}Pb are labeled with “+,” “x,” and “-” signs for groups 1, 2 and 5, respectively.

the total intensity numbers. The $B(M1)/B(E2)$ ratios in Table III are smaller than in the heavier lead nuclei [19,23], but comparable to those in ^{195}Pb [29]. Intensity is feeding into band 1a over the entire spin range, but no depopulation is observed until below the bandhead.

Band 1b is only weakly populated. It decays via unobserved transitions into band 1a. Only four transitions have been assigned to this band. The bandhead spin is estimated to be $47/2 \pm 1\hbar$ from the decay pattern.

Figure 5(a) shows the experimental spins as a function of rotational frequency for band 1a and 1b in ^{193}Pb and for the corresponding bands in other odd-A Pb isotopes [16,23,29,30]. The structure in the lower part is very similar for all bands. The backbending starts at about $\hbar\omega \sim 0.4$ MeV, suggesting a crossing frequency of about 0.3 MeV for all odd-A lead isotopes. The two transitions at the top of band 1a in ^{193}Pb show a sharp upbend, which might be the onset of a second backbending or, perhaps, the band becomes irregular at higher spins. The curve of band 1b as displayed in Fig. 5(a) has approximately the same spin and slope as the upper part of band 1 in $^{197,199}\text{Pb}$ and band 1b in ^{195}Pb suggesting a similar structure.

Figure 4(b) shows a sum of spectra double-gated on the dipole transitions of band 2. These transitions are in coincidence with the transitions of group 2. The connection of this dipole band 2 to the spherical levels has been established, enabling a comparison of experimental and theoretical values. As discussed above, there remains an ambiguity in the spin assignment for band 2, and the parity could not be determined. Only one $E2$ crossover transition has been observed. The $B(M1)/B(E2)$ ratio given in Table III is small compared to the “shears” bands in the heavier lead isotopes [19,23]. The intensity pattern summarized in Table III is similar to that of most of the “shears” bands. There is side-feeding over a wide spin range, but depopulation occurs only in parallel with the lowest transition. The transitions associated with the missing intensity depopulating the (41/2) level could not be observed. The spin versus rotational frequency, $\hbar\omega$, plot [Fig. 5(b)] shows that band 2 follows the systemat-

TABLE III. Spins, transition energies, total intensities, and $B(M1)/B(E2)$ values for dipole bands in ^{193}Pb .

I_{initial} (\hbar)	$E_{\gamma}(E2)$ (keV)	$E_{\gamma}(M1)$ (keV)	$I_{\text{tot}}^{\text{a}}$	$B(M1)/B(E2)$ ($\mu\text{e}b$) ²
Band 1a				
31/2 ⁻		102.5	100.0 ± 17.4	
33/2 ⁻		252.3	99.3 ± 10.5	
35/2 ⁻	633.2	381.2	77.9 ± 9.8	16.4 ± 5.2
37/2 ⁻	782.5	401.3	54.9 ± 7.5	12.8 ± 2.6
39/2 ⁻	814.5	413.3	33.8 ± 5.3	7.9 ± 2.0
41/2 ⁻	747.6	334.4	15.8 ± 3.0	27.9 ± 11.4
43/2 ⁻	691.7	357.4	12.6 ± 3.2	21.6 ± 8.0
45/2 ⁻	710.7	353.3	6.2 ± 2.3	10.0 ± 3.8
Band 1b				
(49/2)		239.1	73.4 ± 19.8	
(51/2)		265.1	100.0 ± 22.0	
(53/2)		329.4	56.1 ± 18.2	
(55/2)		374.9	17.1 ± 7.4	
Band 2				
(41/2)		197.0	46.9 ± 15.0	
(43/2)		232.0	100.0 ± 15.6	
(45/2)		291.4	79.5 ± 12.7	
(47/2)		365.0	61.3 ± 9.8	
(49/2)	753.8	389.1	38.3 ± 7.3	8.2 ± 2.2
(51/2)		415.7	18.7 ± 4.7	
(53/2)		425.7	10.8 ± 3.2	
(55/2)		432.3	6.8 ± 2.5	
Band 3				
29/2 ⁺		342.6	100.0 ± 12.4	
31/2 ⁺	705.9	363.5	91.2 ± 14.6	7.0 ± 1.3
33/2 ⁺	772.8	409.3	53.2 ± 10.6	4.1 ± 0.8
35/2 ⁺	791.1	381.7	30.2 ± 8.4	4.9 ± 1.0

^aTotal intensity of dipole transitions plus intensity of the parallel $E2$ crossover transitions. The intensities are normalized to the strongest band transition.

ics of the strong, positive-parity bands found in the heavier odd-A Pb isotopes [16,23,29,30]. This similarity suggests positive parity for band 2 in ^{193}Pb . While bands 2 in ^{199}Pb and ^{201}Pb show a constant slope, the curve upbends in the lighter isotopes, probably indicating the alignment of additional $i_{13/2}$ neutrons.

Only four transitions have been observed in band 3. They have relatively large intensities and show a less regular energy pattern compared to the other bands in ^{193}Pb . Three crossover transitions have been assigned. Spin and parity could be assigned to this band as it decays directly to the known $27/2^+$ level at 2426 keV. It is possible that the transitions of this band are electric dipoles, but no $E1$ dipole bands have been previously observed in the neighboring lead isotopes. Intensity arguments can exclude $E1$ transitions for the other dipole bands, since these bands have low energy transitions near the bandhead which are strongly converted. For band 3 the $B(M1)/B(E2)$ ratios summarized in Table III are low compared to the other dipole bands in ^{193}Pb .

IV. DISCUSSION

A. Tilted-axis cranking calculations

Lifetime measurements [17–21] of magnetic dipole bands in the Pb isotopes indicate that these bands are built on weakly deformed structures; the oblate character is deduced from negative $E2/M1$ mixing ratios [1,2]. These results are supported by theoretical calculations, including those in the tilted-axis cranking (TAC) framework [23], which indicate that the quadrupole deformation parameter β is in the range $0.05 \leq \beta \leq 0.1$ and $\gamma \approx -70^\circ$ for the bands found in the lead isotopes. For this deformation the highest occupied proton orbital is the $s_{1/2}$ level from which excitations are readily possible across the $Z=82$ gap into the high- K levels of the $h_{9/2}$ and $i_{13/2}$ subshells.

For the neutrons the $i_{13/2}$ subshell is partly filled and holes in the upper levels of this shell contribute to the neutron spin. These are the levels with small K values, and the angular momentum for the neutrons has only a small component in the direction of the nuclear symmetry axis. This means that near the bandhead proton and neutron spins are perpendicular to each other. The total spin is, therefore, tilted to the symmetry axis by an angle of about 45° . Tilted axis cranking (TAC) calculations show that this angle remains nearly constant within the bands. The generation of angular momentum within the bands can be explained by a continuous increase in the alignment of the proton and the neutron spins into the direction of the total spin [22]. At the top of the band both spins are expected to be parallel, resulting in the maximum total spin.

Theoretical calculations of the excitation energies of possible $M1$ band configurations have been performed by applying the semiclassical TAC formalism described in [22]. For simplicity the deformation parameters are kept constant at $\beta=0.1$ and $\gamma=-60^\circ$ as the results of the calculations do not change strongly for slightly varying deformations. The pairing constants were $\Delta=0$ for the protons and $\Delta=0.75$ for the neutrons. The latter corresponds to 80% of the odd-even mass difference, which gives good agreement between theory and experiment in the lead region. The application of the calculations to the very similar isotope ^{199}Pb are de-

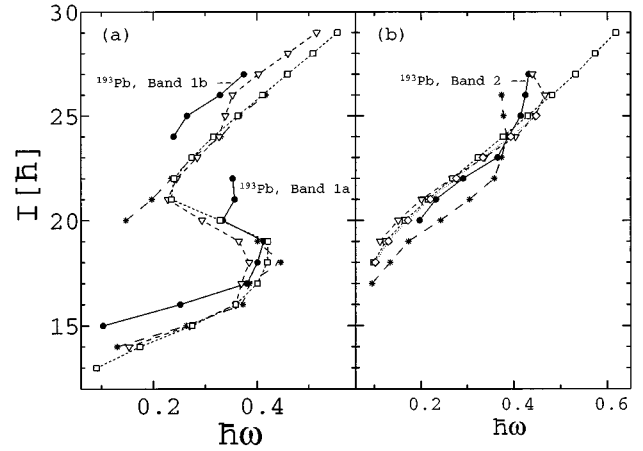


FIG. 5. Experimental spins as a function of rotational frequency for band 1 (a) and band 2 (b) in the odd-A Pb isotopes ^{193}Pb (\bullet), ^{195}Pb ($*$), ^{197}Pb (∇), ^{199}Pb (\square), and ^{201}Pb (\diamond). Values are taken from [16,23,29,30] and the present work.

scribed in more detail in [23]. To compare calculated and experimental values, the classical variable J is associated with the nuclear spin quantum number $I+1/2$ to account for the lowest order quantal corrections. For the transition $I \rightarrow I-1$ the transition energy is associated with $\hbar\omega$ and the classical transition spin $J = \frac{1}{2}[I + (I-1)] + \frac{1}{2} = I$.

B. Configuration assignment

The configurations which we propose to assign to the bands in ^{193}Pb are summarized in Table IV. In this table the nucleon configurations are labeled according to the standard cranked shell model convention. Neutron configurations with positive parity ($i_{13/2}$) are labeled with the letters A, B, C, and D in the order of rising level energy, while negative parity neutron orbitals ($p_{3/2}$ and $f_{5/2}$) are labeled E and F. The proton configurations are only labeled by the total proton spin, for example, 11 for one $h_{9/2}$ and one $i_{13/2}$ protons coupled to 11^- .

There are four points which support the assignments given in Table IV: (i) The systematics of the experimental spins in the odd-A lead isotopes, (ii) the systematics of the bandhead energies, (iii) comparison of TAC calculations with experimental spins and (iv) comparison of calculations with experimental excitation energies within the bands in

TABLE IV. Proposed configurations for dipole bands in ^{193}Pb .

Band	Configuration ^a	Neutrons	Protons
1a	A11	$(i_{13/2}^{-1})13/2^+$	$(s_{1/2}^{-2}h_{9/2}i_{13/2})11^-$
1b	ABC11	$(i_{13/2}^{-3})33/2^+$	$(s_{1/2}^{-2}h_{9/2}i_{13/2})11^-$
2	ABE11	$(i_{13/2}^{-2}p_{3/2}^{-1})27/2^-$	$(s_{1/2}^{-2}h_{9/2}i_{13/2})11^-$
	ABF11	$(i_{13/2}^{-2}f_{5/2}^{-1})29/2^-$	$(s_{1/2}^{-2}h_{9/2}i_{13/2})11^-$
3	A7	$(i_{13/2}^{-1})13/2^+$	$(s_{1/2}^{-1}i_{13/2})7^+$
	A8	$(i_{13/2}^{-1})13/2^+$	$(s_{1/2}^{-2}h_{9/2}^2)8^+$

^aAbbreviations are explained in the text.

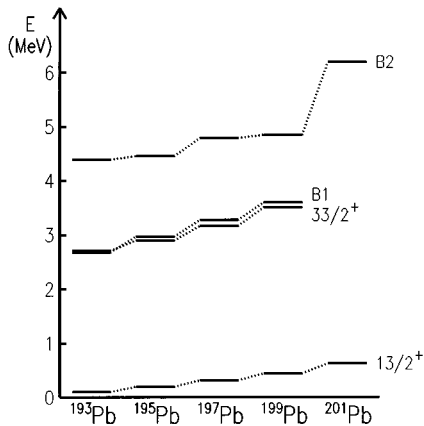


FIG. 6. Odd mass Pb systematics of the bandhead energies of band 1 ($B1$) and band 2 ($B2$) compared to the $13/2^+$ and $33/2^+$ spherical levels. Values are taken from [16,23,29,30] and the present work. The energy of the $13/2^+$ state in ^{193}Pb is estimated to be ≈ 100 keV from systematics. Unknown low energy transitions in ^{199}Pb (below band 2) and in ^{201}Pb ($29/2^- \rightarrow 25/2^-$) are assumed to have 70 keV. The single-particle configurations of the bandheads are given in Table IV; the configurations of the $13/2^+$ and $33/2^+$ levels are $\nu(i_{13/2}^-)$ and $\nu(i_{13/2}^-)$, respectively.

^{193}Pb . The proton ($h_{9/2}i_{13/2}^-$) 11^- configuration is also consistent with earlier lifetime measurements [18].

Figure 5 shows the experimental spins as a function of rotational frequency for band 1 and band 2 in the odd-A Pb isotopes. As already discussed above, the bands show similar properties in all isotopes, which suggests the assignment of the same nucleon configuration to all bands 1 and bands 2, respectively, in the odd-A Pb isotopes. In earlier work [16,23], band 1 has been assigned A11 below the backbend in the heavier isotopes. The configuration ABC11 has been assigned for band 1 above the backbend in $^{197,199}\text{Pb}$ [16,23] and for band 1b in ^{195}Pb [29]. These configurations correspond to one and three $i_{13/2}$ neutron holes (A and ABC in CSM notation), which couple to the 11^- proton configuration to form the “shears” bands. Band 2 has been proposed as ABE11 in $^{195,197,199,201}\text{Pb}$ [29,16,23,30] where the negative parity neutron “E” stems from the $f_{5/2}-p_{3/2}$ orbitals.

In Fig. 6 the bandhead energies of bands 1 and 2 in the odd-A lead isotopes are compared to the energies of the spherical $13/2^+$ and $33/2^+$ levels. The smooth increase of the bandhead excitation energies with increasing neutron number also suggests the assignment of the same nucleon configuration to all bands 1 and bands 2, respectively. The sharp increase of excitation energy for band 2 in ^{201}Pb can be explained by the filling of the $i_{13/2}$ neutron shell in this isotope and, therefore, more energy is necessary to excite neutrons across the shell gap.

Figure 7 shows the experimental spins of the dipole bands in ^{193}Pb versus $\hbar\omega$. The calculated values for all possible configurations are also included in Fig. 7. The experimental values for band 1a, 1b, and band 2 below the upbending are well-reproduced by the calculated values, thus suggesting the configurations A11, ABC11, and ABE11, respectively, which have also been assigned to the corresponding bands in the heavier lead nuclei. Band 2 could also have the configuration ABF11; since the calculated values for this configura-

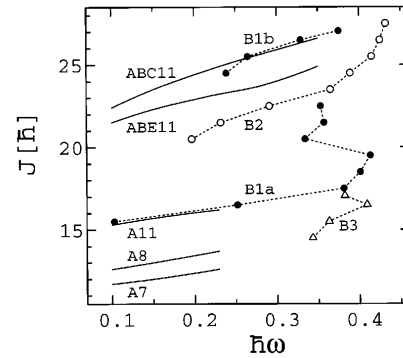


FIG. 7. Experimental and TAC-calculated spins as a function of the rotational frequency, $\hbar\omega$, for the dipole bands in ^{193}Pb . The experimental dipole bands [band 1 below ($B1a$) and above ($B1b$) the backbend, band 2 ($B2$) and band 3 ($B3$)] are indicated by symbols connected by dashed lines. The theoretical calculations (solid lines) are labeled by the configurations listed in Table IV. For band 1b and band 2 the experimental spins have an uncertainty of $\pm 1\hbar$.

tion are similar to those for ABE11 they are not included in the figure. The configurations involving one neutron hole (A) could only be calculated up to 0.23 MeV because at this frequency there is a high level density for neutron orbitals in the Nilsson diagram. This high level density causes irregularities in the calculated energies which originate from competing quasi-neutron configurations. This is different from the calculations in the heavier isotopes, where one may follow the configuration up to much higher frequency [23]. This means that for neutron number around 110 the rearrangement of the neutrons into different quasiparticle configurations competes with the gradual closing of the blades of the shears, resulting in less regular dipole sequences. This aspect will be discussed further in the following section.

Band 3 has lower spin and excitation energy than the other bands. Therefore, the positive-parity configuration A7, in which only one high- j $i_{13/2}$ proton contributes, is a possible assignment for this band. The positive-parity configuration A8, in which two protons are excited in the $h_{9/2}$ orbital, could also explain the properties of band 3 and is, therefore, included in Fig. 7. Band 3 starts at $\hbar\omega=0.34$ while the calculations only provide reliable results up to $\hbar\omega=0.23$; extrapolating the calculated curves does not help to provide an unambiguous configuration assignment of band 3. This band, which lies high in frequency, is not very regular.

In Fig. 8 experimental and calculated excitation energies as a function of J are compared. The experimental values of bands 1a, 1b, and 2 have slopes similar to the calculated values for the proposed configurations. However, there remains an uncertainty in the configuration assignment for band 1b because the absolute excitation energy based on the decay pattern is only a rough estimate. Transitions which link this band to the rest of the level scheme have not been identified. Also in Fig. 8 the experimental values for band 3 are compared with the TAC calculations for the configurations A7 and A8. However, the calculations for both configurations predict a smaller slope than the experimental values.

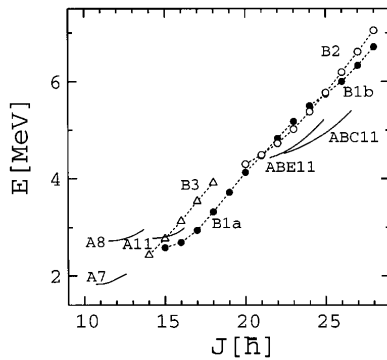


FIG. 8. Experimental and calculated excitation energies as a function of spin for the dipole bands in ^{193}Pb . For band 1b the absolute excitation energy is not known and only roughly estimated from the decay pattern. See also caption to Fig. 7.

C. Regularity of bands

Some of the “shears” bands in the heavier isotopes have been originally interpreted as irregular bands. Due to better statistics in recent experiments the order of the transitions has been reversed in ^{196}Pb [32], ^{197}Pb [16] and ^{198}Pb [33]. This leaves only regular bands in $^{195-202}\text{Pb}$, while there are slightly irregular bands in ^{192}Pb [34], ^{193}Pb and ^{194}Pb [35].

Generally, there is a tendency that the “shears” bands become shorter and less regular with decreasing neutron number. Such a behavior has been found in a shell model study of “shears” bands [31], where it has been attributed to a lack of particles in the $f_{5/2}-p_{3/2}$ orbitals, which serve as a kind of “glue” to fix the two blades of the shears.

The neutron number 112 marks the border between the regions where the neutron system prefers prolate instead of slight oblate deformation (cf., e.g., [36,37]). The lower $B(M1)/B(E2)$ values and the higher $\mathcal{J}^{(2)}$ value of the regular parts of bands 1a and 1b in ^{193}Pb , as compared to the heavier Pb isotopes, may be evidence for the tendency of the neutron system towards prolate deformation. The surprising fact that this leads to *less regular* bands can be understood. TAC calculations show that larger deformation suppresses the “shears” mechanism, because the restoring force that keeps the blades open increases. On the other hand, it becomes easier to generate collective angular momentum from the core nucleons, which do not participate in the shears. In the heavy Pb isotopes the “shears” mechanism is the dominating source of angular momentum [22], generating very regular sequences, whereas in the lighter ones the angular momentum contribution from the deformed core becomes more important. Since the deformation is still rather small, it does not lead to regular bands but rather to irregular quasirotational sequences. An additional element which could destabilize the “shears” mechanism is the change from small

oblate to prolate deformation (cf. [36]), because the deformed field that “glues” the high j particles to the two blades of the “shears” is no longer optimal (cf. the overlap arguments given in Ref. [22]).

V. CONCLUSION

Excitations in ^{193}Pb up to $55/2\hbar$ and 7 MeV in energy were deduced from experiments with early implementation of GAMMASPHERE and HERA arrays of Compton-suppressed Ge detectors using the $^{174}\text{Yb}(^{24}\text{Mg},5n)$ reaction at beam energies of 129, 131, and 134 MeV. The spherical part of the level scheme was considerably extended, which might be helpful in the search of the linking transitions for the superdeformed bands which have been found in this nucleus.

Four bands of enhanced dipole transitions have been observed in ^{193}Pb . Three of these bands have transitions which connect them to the spherical levels, thus enabling a comparison between experimental values and theoretical calculations. The bands are built on configurations involving the high- K proton $h_{9/2}$ and $i_{13/2}$ levels and holes in the low- K levels of the $i_{13/2}$ neutron shell. A comparison of the experimental results with tilted axis cranking (TAC) calculations shows a good agreement for the proposed configurations for bands 1 and 2, while the short, less regular band (band 3) cannot be assigned an unambiguous configuration. Probably band 3 is built on a configuration involving only one high- j proton particle and one high- j neutron hole.

As a result of the present work, the systematics of the $M1$ bands in the odd- A Pb isotopes have been extended. Bands 1 and 2 show a pattern similar to that of the corresponding bands in the heavier lead isotopes, $^{195,197,199,201}\text{Pb}$, thus suggesting that all of these bands are built on the same configurations.

It appears that ^{193}Pb marks the lower borderline of the region of regular “shears” bands in the heavy lead isotopes. This change could be caused by a competition between the neutrons that begin to drive towards prolate deformation below $N=112$ and the closed shell of the proton system that does not allow for large deformation. This competition means that the change in $M1$ character materializes as the appearance of less regular bands instead of more regular ones.

ACKNOWLEDGMENTS

This work has been funded by the National Science Foundation (Rutgers) and by the Department of Energy, under Contract Nos. DE-AC03-76SF00098 (LBL) and W-7405-ENG-48 (LLNL). We want to thank the group in Orsay, France [29] for providing results on ^{195}Pb prior to publication.

[1] R.M. Clark, R. Wadsworth, E.S. Paul, C.W. Beausang, I. Ali, A. Astier, D.M. Cullen, P.J. Dagnall, P. Fallon, M.J. Joyce, M. Meyer, N. Redon, P.H. Regan, W. Nazarewicz, and R. Wyss, *Phys. Lett. B* **275**, 247 (1992).

[2] G. Baldsiefen, H. Hübel, D. Mehta, B.V. Thirumala Rao, U. Birkental, G. Fröhlingdorf, M. Neffgen, N. Nenoff, S.C. Pancholi, N. Singh, W. Schmitz, K. Theine, P. Willsau, H. Grawe, J. Heese, H. Kluge, K.H. Maier, M. Schramm, R. Schubart,

- and H.J. Maier, *Phys. Lett. B* **275**, 252 (1992); *Prog. Part. Nucl. Phys.* **28**, 427 (1992); in *Proceedings of the Xth International School on Nuclear Physics, Neutron Physics and Nuclear Energy*, Varna 1991, edited by W. Andreitschiff and D. Elenkov (Institute for Nuclear Research and Nuclear Energy, Sofia, 1991).
- [3] A. Kuhnert, M.A. Stoyer, J.A. Becker, E.A. Henry, M.J. Brinkman, S.W. Yates, T.F. Wang, J.A. Cizewski, F.S. Stephens, M.A. Deleplanque, R.M. Diamond, A.O. Macchiavelli, J.E. Draper, F. Azaiez, W.H. Kelly, and W. Korten, *Phys. Rev. C* **46**, 133 (1992); *Nucl. Phys.* **A553**, 567c (1993).
- [4] R.M. Clark, R. Wadsworth, E.S. Paul, C.W. Beausang, I. Ali, A. Astier, D.M. Cullen, P.J. Dagnall, P. Fallon, M.J. Joyce, M. Meyer, N. Redon, P.H. Regan, J.F. Sharpey-Schafer, W. Nazarewicz, and R. Wyss, *Z. Phys. A* **342**, 371 (1992).
- [5] G. Baldsiefen, H. Hübel, F. Azaiez, C. Bourgeois, D. Hojman, A. Korichi, N. Perrin, and H. Sergolle, *Z. Phys. A* **343**, 245 (1992).
- [6] N. Roy, J.A. Becker, E.A. Henry, M.J. Brinkman, M.A. Stoyer, J.A. Cizewski, R.M. Diamond, M.A. Deleplanque, F.S. Stephens, C.W. Beausang, and J.E. Draper, *Phys. Rev. C* **47**, R930 (1993).
- [7] J.R. Hughes, Y. Liang, R.V.F. Janssens, A. Kuhnert, J.A. Becker, I. Ahmad, I.G. Bearden, M.J. Brinkman, J. Burde, M.P. Carpenter, J.A. Cizewski, P.J. Daly, M.A. Deleplanque, R.M. Diamond, J.E. Draper, C. Duyar, B. Fornal, U. Garg, Z.W. Grabowski, E.A. Henry, R.G. Henry, W. Hesselink, N. Kalantar-Nayestanaki, W.H. Kelly, T.L. Khoo, T. Lauritzen, R.H. Mayer, D. Nisius, J.R.B. Oliveira, A.J.M. Plompen, W. Reviol, E. Rubel, F. Soramel, F.S. Stephens, M.A. Stoyer, D. Vo, and T.F. Wang, *Phys. Rev. C* **47**, R1337 (1993).
- [8] B. Cederwall, M.A. Deleplanque, F. Azaiez, R.M. Diamond, P. Fallon, W. Korten, I.Y. Lee, A.O. Macchiavelli, J.R.B. Oliveira, F.S. Stephens, W.H. Kelly, D.T. Vo, J.A. Becker, M.J. Brinkman, E.A. Henry, J.R. Hughes, A. Kuhnert, M.A. Stoyer, T.F. Wang, J.E. Draper, C. Duyar, E. Rubel, and J. de Boer, *Phys. Rev. C* **47**, R2443 (1993).
- [9] G. Baldsiefen, U. Birkental, H. Hübel, N. Nenoff, B.V. Thirumala Rao, P. Willsau, J. Heese, H. Kluge, K.H. Maier, R. Schubart, and S. Frauendorf, *Phys. Lett. B* **298**, 54 (1993).
- [10] R.M. Clark, R. Wadsworth, F. Azaiez, C.W. Beausang, A.M. Bruce, P.J. Dagnall, P. Fallon, P.M. Jones, M.J. Joyce, A. Korichi, E.S. Paul, and J.F. Sharpey-Schafer, *J. Phys. G* **19**, L57 (1993).
- [11] P. Dagnall, C.W. Beausang, P. Fallon, P.D. Forsyth, E.S. Paul, J.F. Sharpey-Schafer, P.J. Twin, I. Ali, D.M. Cullen, M.J. Joyce, G. Smith, R. Wadsworth, R.M. Clark, P.H. Regan, A. Astier, M. Meyer, and N. Redon, *J. Phys. G* **19**, 465 (1993).
- [12] R.M. Clark, R. Wadsworth, E.S. Paul, C.W. Beausang, I. Ali, A. Astier, D.M. Cullen, P.J. Dagnall, P. Fallon, M.J. Joyce, M. Meyer, N. Redon, P.H. Regan, J.F. Sharpey-Schafer, W. Nazarewicz, and R. Wyss, *Nucl. Phys.* **A562**, 121 (1993).
- [13] Y. LeCoz, N. Redon, A. Astier, R. Berand, R. Duffait, M. Meyer, F. Hannachi, G. Bastin, I. Deloncle, B. Gall, M. Kaci, M.G. Porquet, C. Schüick, F. Azaiez, C. Bourgeois, J. Duprat, A. Korichi, N. Perrin, N. Poffé, H. Sergolle, J.F. Sharpey-Schafer, C.W. Beausang, S.J. Gale, M.J. Joyce, E.S. Paul, R.M. Clark, K. Hauschild, R. Wadsworth, J. Simpson, M.A. Bentley, A.G. Smith, H. Hübel, P. Willsau, G. de France, S. Ahmad, M. Carpenter, R. Henry, R.V.F. Janssens, T.L. Khoo, and T. Lauritsen, *Z. Phys. A* **348**, 87 (1994).
- [14] P.J. Dagnall, C.W. Beausang, R.M. Clark, R. Wadsworth, S. Bhattacharjee, P. Fallon, P.D. Forsyth, D.B. Fossan, G. de France, S.J. Gale, F. Hannachi, K. Hauschild, I.M. Hibbert, H. Hübel, P.M. Jones, M.J. Joyce, A. Korichi, W. Korten, D.R. LaFosse, E.S. Paul, H. Schnare, K. Starosta, J.F. Sharpey-Schafer, P.J. Twin, P. Vaska, M.P. Waring, and J.N. Wilson, *J. Phys. G* **20**, 1591 (1994).
- [15] M.G. Porquet, F. Hannachi, G. Bastin, V. Brindejone, I. Deloncle, B. Gall, C. Schüick, A.G. Smith, F. Azaiez, C. Bourgeois, J. Duprat, A. Korichi, N. Perrin, N. Poffé, H. Sergolle, A. Astier, Y. LeCoz, M. Meyer, N. Redon, J. Simpson, J.F. Sharpey-Schafer, M.J. Joyce, C.M. Beausang, R. Wadsworth, and R.M. Clark, *J. Phys. G* **20**, 765 (1994).
- [16] G. Baldsiefen, S. Chmel, H. Hübel, W. Korten, M. Neffgen, W. Pohler, U.J. van Severen, J. Heese, H. Kluge, K.H. Maier, and K. Spohr, *Nucl. Phys.* **A587**, 562 (1995).
- [17] T.F. Wang, E.A. Henry, J.A. Becker, A. Kuhnert, M.A. Stoyer, S.W. Yates, M.J. Brinkman, J.A. Cizewski, A.O. Macchiavelli, F.S. Stephens, M.A. Deleplanque, R.M. Diamond, J.E. Draper, F.A. Azaiez, W.H. Kelly, W. Korten, E. Rubel, and Y.A. Akovali, *Phys. Rev. Lett.* **69**, 1737 (1992).
- [18] J.R. Hughes, J.A. Becker, M.J. Brinkman, E.A. Henry, R.W. Hoff, M.A. Stoyer, T.F. Wang, B. Cederwall, M.A. Deleplanque, R.M. Diamond, P. Fallon, I.Y. Lee, J.R.B. Oliveira, F.S. Stephens, J.A. Cizewski, L.A. Bernstein, J.A. Draper, C. Duyar, E. Rubel, W.H. Kelly, and D. Vo, *Phys. Rev. C* **48**, 2135 (1993).
- [19] R.M. Clark, R. Wadsworth, H.R. Andrews, C.W. Beausang, M. Bergstrom, S. Clarke, E. Dragulescu, T. Drake, P.J. Dagnall, A. Galindo-Uribarri, G. Hackman, K. Hauschild, I.M. Hibbert, V.P. Janzen, P.M. Jones, R.W. MacLeod, S.M. Mullins, E.S. Paul, D.C. Radford, A. Semple, J.F. Sharpey-Schafer, J. Simpson, D. Ward, and G. Zwartz, *Phys. Rev. C* **50**, 84 (1994).
- [20] E.F. Moore, M.P. Carpenter, Y. Liang, R.V.F. Janssens, I. Ahmad, I.G. Bearden, P.J. Daly, M.W. Drigert, B. Fornal, U. Garg, Z.W. Grabowski, H.L. Harrington, R.G. Henry, T.L. Khoo, T. Lauritsen, R.H. Mayer, D. Nisius, W. Reviol, and M. Sferrazza, *Phys. Rev. C* **51**, 115 (1995).
- [21] M. Neffgen, G. Baldsiefen, S. Frauendorf, H. Grawe, J. Heese, H. Hübel, H. Kluge, A. Korichi, W. Korten, K.H. Maier, D. Mehta, J. Meng, N. Nenoff, M. Piiparinen, M. Schönhofer, R. Schubart, U.J. van Severen, N. Singh, G. Sletten, B.V. Thirumala Rao, and P. Willsau, *Nucl. Phys.* **A595**, 499 (1995).
- [22] S. Frauendorf, *Nucl. Phys.* **A557**, 259c (1993).
- [23] G. Baldsiefen, H. Hübel, W. Korten, D. Mehta, N. Nenoff, B.V. Thirumala Rao, P. Willsau, H. Grawe, J. Heese, H. Kluge, K.H. Maier, R. Schubart, S. Frauendorf, and H.J. Maier, *Nucl. Phys.* **A574**, 521 (1994).
- [24] M.A. Stoyer *et al.*, *Proceedings of the 205th American Chemical Society*, Denver, Colorado, 1993, part II, abstract NUCL-56; M.A. Stoyer *et al.*, *Bull. Am. Phys. Soc.* **37**, 1321 (1992) and LLNL UCRL-JC-109941-ABS (1992); M.A. Stoyer *et al.*, Contribution to the International Conference on Nuclear Structure at High Angular Momentum, Ottawa, 1992 (unpublished), p. 72.
- [25] H.-Q. Jin, Software package, Oak Ridge National Laboratory (1995).
- [26] J.M. Lagrange, M. Pautrat, J.S. Dionisio, Ch. Vieu, and J. Vanhorenbeeck, *Nucl. Phys.* **A530**, 437 (1991).
- [27] J.O. Newton, F.S. Stephens, and R.M. Diamond, *Nucl. Phys.* **A236**, 225 (1974).

- [28] J.R. Hughes, J. A. Becker, L.A. Bernstein, M.J. Brinkman, L.P. Farris, E.A. Henry, R.W. Hoff, M.A. Stoyer, D.T. Vo, S. Asztalos, B. Cederwall, R.M. Clark, M.A. Deleplanque, R.M. Diamond, P. Fallon, I.Y. Lee, A.O. Macchiavelli, and F.S. Stephens, *Phys. Rev. C* **51**, R447 (1995).
- [29] M. Kaci, M.G. Porquet, F. Hannachi, M. Aiche, G. Bastin, I. Deloncle, B.J.P. Gall, C. Schück, F. Azaiez, C.W. Beausang, C. Bourgeois, R.M. Clark, R. Duffait, J. Duprat, K. Hauschild, M.J. Joyce, A. Korichi, Y. Le Coz, M. Meyer, E.S. Paul, N. Perrin, N. Poffe, N. Redon, H. Sergolle, J.F. Sharpey-Schafer, J. Simpson, A.G. Smith, and R. Wadsworth, *Z. Phys. A* **354**, 267 (1996).
- [30] G. Baldsiefen, P. Maagh, H. Hübel, W. Korten, S. Chmel, M. Neffgen, W. Pohler, H. Grawe, K.H. Maier, K. Spohr, R. Schubart, S. Frauendorf, and H.J. Maier, *Nucl. Phys.* **A592**, 365 (1995).
- [31] S. Frauendorf, J. Reif, and G. Winter, *Nucl. Phys. A* (to be published).
- [32] G. Baldsiefen, H. Hübel, W. Korten, U.J. van Severen, J.A. Cizewski, D. Bazzacco, N.H. Medina, C. Rossi Alvarez, G. Lo Bianco, and S. Signorelli, *Z. Phys. A* (to be published).
- [33] I.M. Hibbert and R. Wadsworth (private communication).
- [34] A.J.M. Plompen, M.N. Harakeh, W.H.A. Hesselink, G. van't Hof, N. Kalantar-Nayestanaki, J.P.S. van Schagen, M.P. Carpenter, I. Ahmad, I.G. Bearden, R.V.F. Janssens, T.L. Khoo, T. Lauritsen, Y. Liang, U. Garg, W. Reviol, and D. Ye, *Nucl. Phys.* **A562**, 61 (1993).
- [35] D. Mehta, W. Korten, H. Hübel, K. Theine, W. Schmitz, P. Willsau, C.X. Yang, F. Hannachi, D.B. Fossan, H. Grawe, H. Kluge, and K.H. Maier, *Z. Phys. A* **346**, 169 (1993).
- [36] S. Frauendorf, F. R. May, and V. V. Pashkevich, in *Proceedings of the International Symposium on Future Directions in Studies of Nuclei far from Stability*, Nashville, Tennessee, 1979, edited by J. Hamilton, E.H. Spejewski, C.R. Bingham, and E.F. Zganjar (North-Holland, Amsterdam, 1980), p. 135.
- [37] C. Roulet, G. Albouy, G. Auger, J.M. Lagrange, M. Pautrat, K.G. Rensfelt, H. Richel, H. Sergolle, and J. Vanhorenbeeck, *Nucl. Phys.* **A323**, 495 (1979).